Climatology of the middle atmosphere in LMDz: Impact of source-related parameterizations of gravity wave drag

A. de la Cámara[1], F. Lott[2], and M. Abalos[1]

[1]National Center for Atmospheric Research, Boulder CO, U.S.A.
[2]Laboratoire de Météorologie Dynamique, IPSL and CNRS, École Normale Supérieure, Paris, France

Key Points:

- Good stratospheric climatology using source-related GW parameterizations
- Gravity wave sources have an impact the annual cycle in the middle atmosphere
- Climate change is not significantly affected by changes in GW sources

Corresponding author: A. de la Cámara, `acamara@ucar.edu`

Abstract

Gravity wave (GW) parameterizations control the mean state and variability of the middle atmosphere in present-day climate models. The most recent parameterizations relate the GWs to their nonorographic sources (fronts and convection), which impacts the annual cycle of the GW drag, and makes the GWs respond to the changing climate. These issues are addressed using the Laboratoire de Météorologie Dynamique Zoom (LMDz) climate model, showing first a climatology of the middle atmosphere in the presence of nonorographic GW sources. The model performance is comparable with that documented in earlier model versions, illustrating that there are no major difficulties in including nonorographic GW sources in models. A twin experiment where the parameterization of GWs has no link with the nonorographic sources is also performed. Provided that in the twin experiment the launched GW stress is very intermittent, its climatology compares reasonably well with the experiment with sources. This illustrates that GW intermittency is a key factor in GW dynamics, but also that the dynamical filtering of the waves by the background flow strongly modulates the significance of the sources. Some impacts of having GW sources on the annual cycle of the zonal mean circulation of the middle atmosphere are nevertheless evident. In a changing climate, the impact of introducing GW sources also seems to be substantially mitigated by the dynamical filtering. The experiments and diagnostics are nevertheless limited in time and to the averaged climatology, respectively, calling for longer tests to measure the impacts on the atmospheric low frequency variability.

1 Introduction

The representation of gravity waves (GW) is critical for the proper representation of the circulations of both the troposphere and the middle atmosphere in general circulation models (GCM). Orographic GWs were the first to be parameterized, their effects helping to reduce biases in the upper tropospheric and lower stratospheric jets [e.g., *Palmer et al.*, 1986; *McFarlane*, 1987; *Lott*, 1999]. Non-orographic GWs produced by convection and fronts have been incorporated thereafter, aiming at reducing very large biases in the stratosphere and mesosphere [e.g., *Manzini et al.*, 1997; *Sassi et al.*, 2002; *Lott et al.*, 2005].

Contrarily to the orographic GWs, for which the source mechanisms are relatively well understood, the mechanisms exciting the nonorographic GWs are less evident [*Fritts and Alexander*, 2003]. For this reason, early parameterizations of the nonorographic GWs have no relation with their sources. Among these parameterizations, the so-called ”globally spectral” ones [*Hines*, 1997; *Warner and McIntyre*, 1996] assume that the GWs follow a saturated spectra, somehow in agreement with observations [*Fritts*, 1989, and references therein]. The good performance of the models that use these schemes [e.g., *Lott et al.*, 2005, and references therein] witnesses that, for gravity waves, the dynamical filtering due to the air density decrease with altitude and the vertical variations of the large scale winds play a central role determining the GW drag (GWD). The globally spectral schemes are also used for the practical reason that they permit the treatment of a large ensemble of waves at a reasonable numerical cost. Nevertheless, the absence of sources in GW parameterizations limit their potential calibration with the growing number of in situ and satellite observations, and is maybe a cause for systematic errors, at least in the Southern Hemisphere spring [*McLandress et al.*, 2012; *de la Cámara et al.*, 2016]. Consequently, many efforts have been made from theoretical, observational and modeling perspectives to understand the mechanisms generating nonorographic GWs. As a result, many climate models now include parameterizations of GWs generated by convection [*Beres*, 2005; *Song and Chun*, 2005; *Lott and Guez*, 2013; *Schirber et al.*, 2014a; *Bushell et al.*, 2015] and by fronts [*Rind et al.*, 1988; *Charron and Manzini*, 2002; *Richter et al.*, 2010] or planetary wave breaking [*Zülicke and Peters*, 2008]. Many of these parameterizations prefer to adopt a ”multiwave” approach rather than a globally spectral one to treat the GWs. For the convective waves this is because it is quite easy to include a diabatic heating into a GW linear equation, and for the fronts we can imagine that some momentum forcing can play the same role triggering GWs. Some parameterizations of GWs evaluate a frontongenesis function to identify GW exciting regions [*Rind et al.*, 1988; *Charron and Manzini*, 2002; *Richter et al.*, 2010], a step that is quite demanding technically. For this reason, and also because there are no closed theories relating such an "ageostrophic" forcing to the GWs potentially produced, *de la Cámara and Lott* [2015] use a simple relation between GWs and fronts that is based on theoretical results on GW emission from potential vorticity anomalies in sheared flows [*Lott et al.*, 2010, 2012a]. Interestingly, *de la Cámara et al.* [2016] have recently demonstrated that the GW intermittency resulting from the introduction of sources (convection and fronts) is significant to predict well the timing of the Southern Hemisphere stratospheric final warming. Finally, it is also worthwhile to recall that by using stochastic techniques, the multiwave methods can be made much more computationally efficient than initially thought (see discussions in *Eckermann* [2011]; *Lott et al.* [2012a]).

A fundamental motivation to relate the GWs to their potential sources is that these sources can have an annual cycle and change when the climate change. It is therefore important to test if this can affect the model annual cycle in the middle atmosphere and to analyze if the changes in the GW sources impact the prediction of the future climate. To have a more thorough understanding of their impact, a longer term objective is to include the GW sources in some of the models participating into the next climate model intercomparison project (CMIP6). This is the approach followed by the Laboratoire de Météorologie Dynamique Zoom (LMDz) GCM where all the parameterized GWs will be related to their sources, e.g. mountains, convection and fronts. This is in opposition with CMIP5 [*Lott et al.*, 2005], where the LMDz model used the *Hines* [1997]'s globally spectral scheme to parameterize the nonorographic GWs. The first purpose of this paper is therefore to carefully analyze the model middle atmospheric climate and variability, and to see if the frontal and convective GWs can do at least as well as the *Hines* [1997]'s uniform background of waves. The second is to start testing if having time and space varying sources influences the troposphere and middle atmosphere climate.

The paper is organized as follows. Section 2 presents the LMDz model and summarizes the source-related GW parameterizations. Section 3 validates the model climatology and variability of the middle atmosphere against the European Centre for Middle-range Weather Forecast Interim Reanalysis (ERA-Interim), while section 4 addresses the impact of introducing nonorographic GW sources in the parameterizations. The main conclusions are given in section 5.

2 Model description

The version of LMDz we use has a $3.75^\circ \times 1.875^\circ$ longitude-latitude grid, and 71 levels in the vertical with the top at 0.01 hPa. Its vertical resolution is around 1 km in the lower stratosphere. The results shown are from a 20-year simulation (referred to as CONTROL), forced with climatological fields of sea surface temperature, sea ice, soil temperature and composition over land. These climatological fields are averages over the period 1979-2005, as are the ozone fields, which are those predicted by the LMDz-Reprobus coupled climate-chemistry model [*Jourdain et al.*, 2008].

2.1 Gravity wave drag parameterizations

LMDz uses three distinct GWD parameterizations that account for GWs generated by topography [*Lott*, 1999], convection [*Lott and Guez*, 2013], and fronts [*de la Cámara and Lott*, 2015]. The parameterizations of nonorographic GWs are based on the stochastic approach introduced by *Eckermann* [2011] and *Lott et al.* [2012b], and consists in sampling randomly the GW spectrum by launching 8 monochromatic waves at each grid point and "physical" time step (e.g. every 30 min). The waves chosen are purely zonal, and their zonal wavenumber k is chosen randomly between two extrema corresponding to wavelength between 1km and 300km and using a uniform statistics. The phase speed is chosen randomly according to a Gaussian distribution with 40 m·s^{-1} standard deviation and centered on the wind velocity at the emission level (500 hPa for convective waves, 900 hPa for frontal waves).

As the sensitivity to the non-orographic sources is our first objective, we next recall how this is done in LMDz (for the other aspects, like the treatment of the breaking, or the statistical superposition of the waves see *Lott and Guez* [2013] and *de la Cámara and Lott* [2015]. For convective waves, the emitted GW stress at the launching altitude (z_l) is:

$$\vec{F}^{z_l}_{conv} = \rho_r G_{c0} \left(\frac{R L_W}{\rho_r H c_p} \right)^2 \frac{|\vec{k}|^2 e^{-m^2 \Delta z^2}}{N \Omega^3} P^2 \frac{\vec{k}}{\|\vec{k}\|}, \tag{1}$$

where ρ_r is the density at a reference level, G_{c0} is a tunable, dimensionless parameter of order 1 (we take , $G_{c0} = 1.75$), Δz a tunable characteristic depth of the heating source (we take $\Delta z = 1$ km, R is the ideal gas constant, L_W is the latent heat of condensation, $H = 7$ km is the stratospheric scale height, c_p is the specific heat at constant pressure, $\vec{k}$ is the horizontal wavenumber vector, m is the vertical wavenumber ($m^2 = N^2|\vec{k}|^2/\Omega^2$), N is the buoyancy frequency, $\Omega = \omega - \vec{k} \cdot \vec{U}$ is the intrinsic frequency, and P is the grid-scale precipitation. Therefore, Eq. 1 translates the gridscale precipitation into a subgrid scale GW stress.

For frontal waves, the emitted GW stress is [see *de la Cámara and Lott*, 2015]:

$$\vec{F}^{z_l}_{fron} = G_{f0} \frac{\delta z}{4f} \frac{\vec{k}}{\|\vec{k}\|} \int_0^{z_{top}} \rho_0(z') N(z') \zeta^2(z') e^{-\pi \frac{N(z')}{U_z(z')}} \mathrm{d}z', \tag{2}$$

where G_{f0} is a tunable, dimensionless parameter of order 1 (we take $G_{f0} = 2$), δz is the vertical depth of the vorticity anomaly (set to 1 km), $\rho_0 = \rho_r e^{-z/H}$ is the reference state density, ζ is the grid-scale relative vorticity , and U_z is the vertical shear. As we see Eq. 2 translates the resolved dynamics (gridscale vorticity and stability conditions) into a subgrid scale GW stress.

2.2 Characteristics of the non-orographic gravity waves

Figure 1 shows the annual cycle of eastward and westward momentum flux (MF) at the launching altitude, 100 hPa and 1 hPa. At the level of emission (Fig. 1e,f), the band of high MF in the tropics is due to the convectively generated GWs. The bands in the mid-latitudes of both hemispheres are mainly due to frontal GWs, although convective GWs also contribute. The emitted MF is almost similar in amplitude for eastward and westward MF, and both exhibit a pronounced annual cycle. The tropical band migrates northward and gets stronger during the northern summer, consistent with the behavior of precipitation in the model (not shown). In the midlatitudes, the emitted MFs are weaker than in the tropics and present higher values in winter of both hemispheres, consistent with stronger baroclinicity.

The effect of wind filtering on the GW propagation is evident, the MF getting smaller and smaller when entering the stratosphere at 100 hPa and the mesosphere at 1 hPa. At 100 hPa (Fig. 1c,d), the MF still has some pattern similarities with the emitted MF, although the wind filtering enhances the annual cycle. At 1 hPa (Fig. 1a,b) the tropical band has been filtered out to a large extent. In the extratropics, while the annual cycle pattern of westward MF somehow resembles that of the emitted flux, the pattern of eastward fluxes is almost in phase opposition with that emited, presenting larger values during the summer months in both hemispheres.

It is interesting to compare the GW stress at 100 hPa with the results of *Richter et al.* [2010], where the authors show similar plots for convective and frontal GW stresses separately at 100 hPa in WACCM3.5 (their Figs. 2 and 3). The annual cycle of the GW stress in the tropics (Fig. 1c,d) resembles the convective GW stress in *Richter et al.* [2010], but the magnitude in our model is smaller by a factor of 2. At mid-to-high latitudes, the GW stress at 100 hPa is also qualitatively similar to the frontal GW stress in *Richter et al.* [2010], and this time the magnitude is smaller in our scheme by a factor of $\sim$1.5. Such differences in stress amplitude are not surprising given that the two models are very different, and most of all the WACCM model top (0.0001 hPa) is much higher than the LMDz model top (0.01 hPa), meaning that a given stress can give much larger drag near the top in the first model than in the second. This can yield modelers to tune the launched GW stress to control the drag amplitude near models top.

Figure 2 presents the drag imposed on the mean flow by the frontal, convective, and orographic GW parameterizations for DJF and JJA. Frontal GWs are the main contributor to the total GWD in the southern extratropics in both seasons, with peak values larger than ± 21 m$\cdot$s$^{-1}\cdot$d^{-1} near 60°S at mesospheric levels above 0.1 hPa. Convective GWD is weaker than the frontal drag in the extratropics, but it presents relative maxima (about $\pm$3-6 m$\cdot$s$^{-1}\cdot$d^{-1}) near 50° latitude in both hemispheres at the highest altitudes of the model, presumably associated with the location of the storm tracks. The strong dissipation of MF in the tropics between 100 and 1 hPa described in Fig. 1 is not evident here due to density effects, i.e. the drag is proportional to the the vertical divergence of the momentum flux and inversely proportional to density. Orographic GWD is mainly active in northern winter extratropical stratosphere, reaching -9 m$\cdot$s$^{-1}\cdot$d^{-1} at 0.1 hPa.

3 Mean climate and variability of the middle atmosphere

3.1 Zonal mean climate

As this paper focuses on the impact of including sources in the nonorographic GWD schemes, we have tuned these parameterizations to ensure that LMDz has a climatology at least comparable to that documented in its previous stratospheric version [*Lott et al.*, 2005]. As we shall see, the improvements in some places are obvious, like in the QBO region, whereas in the midlatitudes the effects are more neutral. Note that having a model version with GW sources and a QBO but without degrading the model in other places was an implicit objective of this paper.

To illustrate this, Fig. 3 shows the seasonal averages of zonal-mean zonal wind profiles. It shows well-defined polar night jets in the solstices with values up to 40 and 85 m$\cdot$s^{-1} in the boreal and austral jet cores, respectively. The summer easterly jets present maximum values of -70 m$\cdot$s^{-1} in the subtropics at around 1 hPa, and the winds show transition conditions in the equinoxes. This zonal mean winds compare well with those corresponding to an earlier model version (Fig. 3 in *Lott et al.* [2005]), but some biases that were present in the previous version of the model remain. When compared to ERAI in Fig. 4 we see that the largest biases in the model are in the summer easterly jets, with winds 20 m$\cdot$s^{-1} stronger in LMDz than in ERAI. Also, the SH easterly jet in DJF splits into two parts (Fig. 3a).The strength of the polar night jet is comparable in the two datasets, although the boreal jet in LMDz is weaker than in ERAI in the upper stratosphere and lower mesosphere. This is more clearly seen in Fig. 5, which specifically shows the wind speed in the jet core and its latitudinal position as a function of height during the northern and southern winters. The latitudinal tilt of the jets with altitude is well captured, with the exception of the southern jet in JJA. This bias is common to most climate models [*Butchart et al.*, 2011]. The model performance in MAM and SON shows good agreement with ERAI (Figs. 3 and 4).

To complete the description of the zonal mean circulation, the contours in Fig. 3 display the mass streamfunction in CONTROL, representing the residual mean meridional circulation Ψ^*_{res}:

$$\frac{\partial \Psi^*_{res}}{\partial z} = -\rho_0 \cos\phi\, \bar{v}^*, \tag{3}$$

where $\rho_0 = \rho_0(z)$ is the background density, ϕ is latitude, and $\bar{v}^*$ is the latitudinal component of the residual circulation in the Transformed Eulerian Mean (TEM) formalism [*Andrews et al.*, 1987]:

$$\bar{v}^* \equiv \bar{v} - \frac{1}{\rho_0}\frac{\partial}{\partial z}\left(\frac{\rho_0 \overline{v'\theta'}}{\partial\bar{\theta}/\partial z}\right) \tag{4}$$

In DJF and JJA (Fig. 3c), the main circulation cell presents upward motions in the tropics, extending to the summer hemisphere, that reach mesospheric altitudes, and downward motions in the winter high latitudes. The meridional motion in the mesosphere above 1 hPa is responsible for the dynamical maintenance of winter pole temperatures much warmer than summer pole temperatures in the mesosphere (not shown). A secondary, shallow circulation cell can also be seen in the summer hemisphere lower stratosphere. All these features compare well with ERAI (Fig. 4). During MAM and SON the circulation cells grow deeper in the autumn and shallower in the spring hemispheres, in good agreement with the reanalysis.

3.2 Interannual variability

To analyze the simulated variability, Fig. 6 shows the amplitude and latitudinal location of maximum interannual variability of the polar night jets as a function of height, for CONTROL and ERAI (note that Figs. 5 and 6 include results for GWLOG, which will be discussed in Section 4). For the Northern Hemisphere (NH) winter, the amplitude of the maximum variability is well represented below 1 hPa as compared to ERAI, but the model underestimates it in the lower mesosphere (Fig. 6a). The latitudinal location of this variability is not so well represented (Fig. 6b). While in ERAI the position tilts equatorward with height between 30 and 1 hPa, in LMDz it tilts poleward. This bias is common to many climate models, and needs further investigation [*Butchart et al.*, 2011]. For the Southern Hemisphere (SH) winter, the comparison to ERAI provides similar conclusions. A slight equatorward tilt with height of the maximum variability does appear in CONTROL below 1 hPa, but with a much steeper slope than in ERAI. The maximum variability is 10-20 degrees poleward in CONTROL as compared to ERAI, possibly due to differences in the locations of the jet (Fig. 5d).

A complementary view of the interannual variability is given by the time series of polar temperature in both hemispheres at 10 hPa in Fig. 7. The seasonal evolution and variability, as well as the inter-hemispheric contrasts, are generally well captured. However the model presents too much variability, as evidenced by sporadic warmings in October and November in the North Pole (Fig. 7a), or the spread in temperatures in the South Pole during the austral winter/spring that are not present in the ERAI data. Figure 8 further shows an histogram of frequencies of major sudden warmings (MSW) in the NH for both CONTROL and ERAI, sorted by winter month. We have followed the method by *Charlton and Polvani* [2007] to identify these events. The frequency of events is higher in CONTROL than in ERAI (0.76/year versus 0.67/year), confirming larger simulated variability. Importantly, the intraseasonal distribution of major warmings consistently presents higher frequencies as the winter season progresses, peaking up in February. The differences with ERAI include too high frequencies in November and February, and too low in December. Given the multiple factors influencing the occurrence of MSWs, we consider that the performance of LMDz compares well with that of the previous model version (not shown here, but see Fig. 13 in *Lott et al.* [2005]). Additionally, the model does not present a significant delay in the simulation of the stratospheric final warming in the SH [*de la Cámara et al.*, 2016], a bias that most climate models still have [e.g., *Butchart et al.*, 2011; *McLandress et al.*, 2012; *Wilcox and Charlton-Perez*, 2013].

In the tropical lower stratosphere, the QBO dominates the interannual variability of the zonal winds. Figure 9 shows the zonal winds at the Equator as a function of time and height. The model internally generates a QBO with an average period of 28 months that closely matches that in ERAI (27 months). Yet there are some discrepancies between the model and the reanalysis in Fig. 9, such as wind velocities that are up to 10 m$\cdot$s^{-1} weaker in the model, especially during the westward phase. Also the QBO in CONTROL does not descend as low as it does in ERAI, and it lacks the westerlies stalling that often occurs below 30 hPa (see for example the years 2009-2010 in Fig. 9b). The causes are multiple, but we suspect that the underestimation of the slow Kelvin waves in LMDz might play a significant role [*Maury et al.*, 2013]. The reader is referred to *Lott and Guez* [2013] for further details on the simulation of the QBO in LMDz and the comparison with observations. For completeness, we recall here that the QBO was absent in *Lott et al.* [2005].

4 Impact of source-varying GWD parameterizations

In this section we evaluate the impact of including sources of nonorographic gravity waves (NGW). First, we describe the twin experiments performed, and then we will present the results, with the focus on the simulated annual cycle in the middle atmosphere, and on possible impacts under future climate conditions.

4.1 Model experiments

Recent studies have shown that linking the parameterized GW amplitudes to their nonorographic sources naturally produces extremely intermittent MFs, the distribution of absolute momentum fluxes fitting a lognormal distribution [*de la Cámara et al.*, 2014; *de la Cámara and Lott*, 2015; *Stephan and Alexander*, 2015]. These studies also suggest that the NGW intermittency can help reducing model biases, simply because for a given averaged launched momentum flux, few large amplitude waves break at lower altitude than a large number of small amplitude wave. Therefore, to evaluate the role of the NGW sources specifically, we next replace the source terms in the convective and frontal schemes (i.e. the P^2 and ζ^2 terms in eq. 1 and 2) by random numbers produced by a lognormal distribution. The characteristics of the distribution is tuned to obtain a reasonable zonal mean climatology (see next section). This run is referred to as GWLOG. We also apply a latitudinal weighting in the modified convective GW scheme to launch larger stress in the tropics and help generate a QBO. Specifically, the latitudinal weighting function chosen is $f_w(\phi) = (0.15\sin^2 2\phi + 1.1\cos^{30}\phi)$. This function has a narrow maximum at the equator and two secondary peaks at 45° latitude, qualitatively mimicking the averaged the latitudinal distribution of precipitation [e.g., *Lott and Guez*, 2013]. The magnitudes of the maxima have been chosen *ad hoc* to obtain a reasonable climatology (see net section).

A different potential impact of having source-related NGW schemes is that parameterized wave amplitudes will change if climate changes. To investigate this point, we perform two additional experiments. First we make a 20-year experiment, named 4xCONTROL, where the GW specifications are as in CONTROL, but increasing the CO_2 concentrations by a factor of four, and by adding everywhere 4 K to the prescribed SST. Second we make another 20-year experiment, named 4xGWLOG, similar to 4xCONTROL but using the GW specifications of GWLOG.

4.2 Climatology of the simulation without GW sources

To make a fair comparison between the simulations with and without NGW sources we have tried to make them as close as possible in terms of the GW drag in the mid-latitudes, the middle atmosphere jets in the mid-latitudes and subtropics, and the QBO in the tropical lower stratosphere. Figure 10 displays the nonorographic GWD for DJF and JJA in the CONTROL and GWLOG runs. The lognormal distributions of emitted GW stress used in GWLOG provide GWD profiles qualitatively similar to those in CONTROL. Gravity wave drag values larger than ± 3 m·s^{-1}·d^{-1} are found above 1 hPa in the mesosphere of the two runs. Quantitatively, the drag in CONTROL is slighter weaker than in GWLOG, particularly in the summer hemisphere.

Concerning the impacts on the mean climate, we return to Fig. 5 that shows the strength and location of the wintertime polar jets in GWLOG. The zonal mean climate of GWLOG is comparable to that of CONTROL during the solstices. Although the panels in Fig. 5 focus on the summer easterly and winter westerly jets, essentially because the GW parameterizations are first intended to improve them, it is important to say that similarities are found in the mid-latitudes during other seasons. Beyond the zonal means, it is much more difficult to control the variability, as illustrated in Fig. 6 where the variability of the jet in GWLOG is also shown. The most notorious differences appear in the SH, such as larger variability of the jet in GWLOG (Fig. 6c), and the absence of the equatorward tilt with height in the jet variability below 1 hPa (Fig. 6d).

Still concerning the variability but coming back to the NH, Fig. 8 also shows the MSW statistics for GWLOG. The mean winter frequency is reasonable (0.58 per year), but GWLOG fails in capturing the intraseasonal distribution of the major warmings. This result may be due to chance, but it is interesting that removing the relation with the NGW sources degrades the SSW seasonality. We nevertheless need to test it with longer model simulations.

Finally, and concerning the tropical region, the Fig. 9 shows that GWLOG also has an internally generated QBO, its period is slightly longer than in CONTROL. Above the QBO region, the semi-annual signal seems more pronounced in GWLOG.

4.3 Impact on the annual cycle

We showed in Fig. 1 that the GW stress emitted in CONTROL presents a strong annual cycle, presumably due to the annual cycle of the GW sources activity. Figure 11 presents the eastward and westward NGW stress as a function of latitude and time of the year for GWLOG. As expected, a very weak seasonality appears at the altitude of emission since NGW sources are not considered in this run. At 100 hPa, seasonal differences start to show up, and at 1 hPa a strong annual cycle is present due to momentum flux dissipation. We can now compare this performance in GWLOG with that in CONTROL (Fig. 1). At 1 hPa both eastward and westward momentum fluxes are very similar in magnitude and seasonal evolution in both runs. This contrasts with the stress at 100 hPa, where the annual cycle is much stronger and peak values are much larger for CONTROL than for GWLOG, specially for the westward direction (e.g., 2.1 versus 1.2 mPa at $\sim$50°S in August). It can be interpreted then that the GW stress entering the mesosphere in our simulations is only weakly dependent on the seasonal cycle of the stress at lower altitudes, and in particular on the seasonal cycle introduced by the GW sources. On the other hand, this implies a distinct momentum flux dissipation in the stratosphere between these two runs, which may result in differences of GW drag in the stratosphere.

In terms of nonnorographic GW drag, the difference between CONTROL and GWLOG is also significant as illustrate the Fig. 12a- 12b where the annual cycle of the drag averaged for the northern (50°N-80°N) and southern (50°S-80°S) high latitudes, are shown. In the NH (Fig. 12a), there is a band of negative differences in the lowermost stratosphere during the whole year, perhaps pointing to larger westward net stress emitted (i.e. producing a negative drag) in CONTROL than in GWLOG. Above 50 hPa, a marked seasonal cycle appears, with positive differences during summer and negative during winter, changing sign in the mesosphere above 0.5 hPa. In the SH (Fig. 12b), there is a noticeable annual cycle in the drag up to 0.1 hPa, with positive differences in summer and negative in winter. The magnitude is also small, reaching up to -0.3 $\mathrm{m\cdot s^{-1}\cdot d^{-1}}$ in the upper stratosphere in JJA. The negative differences during the summer months descend throughout the season and reach the lower stratosphere by September.

The impact of the GW seasonality on the annual cycle of the zonal winds at mid-latitudes is not very significant, consistently with the fact that we tuned GWLOG with this objective (see supplementary material). The situation is somehow different if we look at the Brewer-Dobson circulation, as we show below. To evaluate the impact of the GWs on the Brewer-Dobson circulation we use the TEM formalism, where the zonal momentum equation is given by [*Andrews et al.*, 1987]:

$$\frac{\partial \bar{u}}{\partial t} - \bar{v}^* \hat{f} + \bar{w}^* \frac{\partial \bar{u}}{\partial z} = \mathrm{DF} + \bar{X} \tag{5}$$

and where $(\bar{v}^*, \bar{w}^*)$ are the meridional and vertical components of the TEM residual circulation, $\hat{f} = f - \frac{1}{a\cos\phi}\frac{\partial(\bar{u}\cos\phi)}{\partial\phi}$ with f the Coriolis parameter, $\mathrm{DF} = \frac{\vec{\nabla}\cdot\vec{F}}{\rho_0 a\cos\phi}$ is the force applied by the resolved waves with $\vec{F}$ the Eliassen-Palm (EP) flux, and $\bar{X}$ is the force applied by unresolved processes (in our case the parameterized gravity wave drag). In Eq. 5, the left-hand terms represent the circulation response to the forcing applied by the right-hand terms. We next evaluate the vertical motion over the high latitudes (i.e. downwelling), focusing on the possible response of the mean meridional circulation to the NGW drag differences between CONTROL and GWLOG. Following *Randel et al.* [2002] and *Abalos et al.* [2012], we combine Eq. 5 and the TEM continuity equation [*Andrews et al.*, 1987] to derive the vertical component of the residual circulation:

$$\bar{w}^*_m(\phi, z) = \frac{-e^{z/H}}{\int_{\phi_1}^{\phi_2} a\cos\phi\,\mathrm{d}\phi}\left\{\int_z^\infty \frac{e^{-z'/H}\cos\phi}{f(\hat{\phi}, z')}\left[\mathrm{DF}(\phi, z') + \bar{X}(\phi, z') - \frac{\partial\bar{u}(\phi, z')}{\partial t}\right]\mathrm{d}z'\right\}_{\phi_1}^{\phi_2}. \tag{6}$$

We take $\phi_1 = 60°$N, $\phi_2 = 80°$N for the NH, and $\phi_1 = 80°$S, $\phi_2 = 60°$S for the SH. Note that the forcing from the total GW drag (orographic plus non-orographic, i.e. $\bar{X}$) is explicitly taken into account in Eq. 6.

The panels in the second row of Fig. 12 show the annual evolution of the differences of $\bar{w}^*_m$ in the northern and southern high-latitudes. In the NH (Fig. 12c), the pattern is similar to that of the NGWD (Fig. 12a). The fact that the patterns in $\bar{w}^*_m$ are found at lower altitudes than those in the NGWD is consistent with Eq. 6, which links the vertical motion to the drag at that level and above. We see positive differences in the winter mesosphere and negative differences in the summer mesosphere (note that the regions of statistical significant differences are somewhat limited). This means that the amplitude of the annual cycle of $\bar{w}^*_m$ is around 10% weaker in CONTROL than in GWLOG in the mesosphere, and around 10% stronger in the lower stratosphere (note that in the lower stratosphere the value is not statistically significant). In the SH, the differences in $\bar{w}^*_m$ do not present a clear pattern and are barely significant.

To address whether the $\bar{w}^*_m$ differences in the NH between CONTROL and GWLOG emerge from the NGWD differences, we evaluate separately the contributions from the NGWD and from the resolved forcing (i.e. DF in Eq. 5) to the vertical component of the residual circulation [*Hines*, 1991]. We do so by computing $\bar{w}^*_m$ using NGWD alone (i.e. $\bar{w}^*_{m,\mathrm{NGWD}}$):

$$\bar{w}^*_{m,\mathrm{NGWD}}(\phi, z) = \frac{-e^{z/H}}{\int_{\phi_1}^{\phi_2} a\cos\phi\,\mathrm{d}\phi}\left\{\int_z^\infty \frac{e^{-z'/H}\cos\phi}{f(\hat{\phi}, z')}\,\bar{X}_{\mathrm{NGWD}}(\phi, z')\,\mathrm{d}z'\right\}_{\phi_1}^{\phi_2}, \tag{7}$$

and using the divergence of the EP flux alone (i.e. $\bar{w}^*_{m,\mathrm{DF}}$):

$$\bar{w}^*_{m,\mathrm{DF}}(\phi, z) = \frac{-e^{z/H}}{\int_{\phi_1}^{\phi_2} a\cos\phi\,\mathrm{d}\phi}\left\{\int_z^\infty \frac{e^{-z'/H}\cos\phi}{f(\hat{\phi}, z')}\,\mathrm{DF}(\phi, z')\,\mathrm{d}z'\right\}_{\phi_1}^{\phi_2}, \tag{8}$$

The corresponding plots for $\bar{w}^*_{m,\mathrm{NGWD}}$ and $\bar{w}^*_{m,\mathrm{DF}}$ are shown in the third and bottom rows, respectively, of Fig. 12. In the NH, the main contribution to the change in vertical motion is due to the changes in NGWD (Fig. 12e). The differences in $\bar{w}^*_{m,\mathrm{NGWD}}$ strongly resemble in both magnitude and evolution those in $\bar{w}^*_m$, while no clear pattern is observed for $\bar{w}^*_{m,\mathrm{DF}}$.

In the SH, the $\bar{w}^*_{m,\mathrm{NGWD}}$ pattern agrees with the pattern in the forcing (Figs. 12b and 12f). Interestingly, the residual circulation induced by the resolved forcing opposes almost exactly (Fig. 12h) that induced by the NGWD, resulting in the insignificant $\bar{w}^*_m$ differences in the SH. We interpret that in the NH the amplitude and variability of the resolved waves are sufficiently large not to be sensitive to the rather small differences in the annual cycle of the NGWD. In contrast, in the SH the amplitude and variability of the resolved waves are not as large, and they respond compensating the forcing from the parameterized NGWs.

4.4 Impact on a warmer climate

In this section we analyze the potential impact of NGW with source-depending amplitudes on a warmer climate. Figure 13 displays sea level pressure (SLP) differences 4xCONTROL-CONTROL and 4xGWLOG-GWLOG, in DJF (NH) and SON (SH). The tropospheric circulation response to warmer conditions reinforces the subtropical anticyclones and deepens the subpolar lows in both hemispheres, in agreement with projections from the Coupled Model Intercomparison Project Phase 5 (CMIP5) [e.g., *Manzini et al.*, 2014]. The magnitude and locus of the SLP differences look insensitive to the use of parameterized NGW hooked to their sources.

Figure 14 shows the difference between 4xCONTROL and CONTROL in eastward and westward stress at the launching altitude, 100 and 1 hPa. Interesting features emerge in this figure. At the launching level (Figs. 14e, f), there is a poleward shift of the latitude bands with maximum stress in the extratropics of both hemispheres. This is consistent with the intensification of the circulation described in Fig. 13, and with the projected poleward shift in the storm tracks [*Scaife et al.*, 2012]. It can also be seen that the annual cycle intensifies. The poleward shift is also present at 100 hPa (Figs. 14c, d), where the extratropical annual cycle is notably enhanced, particularly for the westward stress. At 1 hPa (Figs. 14a, b), there is a weak reduction in eastward stress, and the enhanced annual cycle in the SH westward stress is collocated with the maximum stress in CONTROL (Figs. 1 b).

Figure 15 shows the corresponding plots for the difference between 4xGWLOG and GWLOG, where we can look into the effect of wind filtering alone. At the launching level (Figs. 15e, f), there is again a poleward shift . However, there is practically no signal of an annual cycle. This implies that the enhanced annual cycle in 4xCONTROL is due to changes in the strength of GW sources, while the poleward shift is due to a shift in the winds and storminess due to warmer conditions. The change in the strength of the annual cycle at 1 hPa, more pronounced for the westward component of the momentum flux (Fig. 15b), is mainly a result of changes in the wind filtering, and not of changes in the sources.

We next analyze the potential impact of triggering GWs from their sources on the seasonal cycle of the downwelling branches of the Brewer-Dobson circulation in a warmer climate. Figure 16 presents similar plots as Fig. 12, but for the difference 4xCONTROL minus 4xGWLOG. The change in the NGW drag induced by linking the wave amplitude to their sources is very similar in warmer and in present climate conditions in both structure and magnitude (compare Fig. 16a, b, and Fig. 12a, b). This similarity appears also in the $\bar{w}^*_m$, $\bar{w}^*_{m,\mathrm{NGWD}}$, and $\bar{w}^*_{m,\mathrm{DF}}$ responses. Interestingly, some statistically significant changes in $\bar{w}^*_{m,\mathrm{DF}}$ show up in the NH (Fig. 16g), but contrarily to what happens in the SH, they have the same sign as $\bar{w}^*_{m,\mathrm{NGWD}}$ (Fig. 16c). We can then conclude that the self-adjustment of parameterized NGW amplitudes to climatological changes in the sources has a minor effect on the induced middle-atmospheric circulation changes in a warmer climate. We have just discussed the impact on the extra-tropical downwelling because we find it to be the most sensitive aspect of the mid-latitude circulation to respond to the GWs annual cycle. We nevertheless verified that this conclusion also applies to the zonal winds, and found that the differences between 4xCONTROL and 4XGWLOG in zonal mean zonal winds are almost identical to those betwen CONTROL and GWLOG (not shown but see supplementary material).

In the tropics, the situation is not as clear, and it is more difficult to deliver a clear message. We find significant changes in the amplitude and period of the QBO between 4xCONTROL and 4xGWLOG. In both runs the QBO period decreases drastically and the amplitude of the eastward phase is reduced. Also, in 4xGWLOG the oscillation of the winds is lost below 20 hPa, remaining in westward phase (see supplementary material). Nonetheless, different settings and tuning of a given parameterization may have different -and somewhat inconsistent- QBO responses in simulations of a warmer climate [*Schirber et al.*, 2014b], so we do not consider that those changes be due to a crucial role of the GW sources.

5 Summary and Concluding Remarks

In this work, we present the mean climate and variability of the middle atmosphere in the new version of the LMDz general circulation model. A novel characteristic of LMDz is that it includes a set of gravity wave parameterizations where the emitted stress is linked to the source characteristics, namely flow over topography, convection, and fronts and jet imbalances. In general, LMDz with source-related GWD (i.e. CONTROL) shows good climatology and interannual variability as compared to ERA-Interim. Some well-known biases persist, as the lack of an equatorward tilt with height of the southern stratospheric polar night jet, and too strong summer easterly jets in both hemispheres. The model presents good statistics of sudden stratospheric warmings, and internally generates a QBO in the tropical stratosphere with reasonable amplitude and mean period, as described in more detail by *Lott and Guez* [2013].

There are two major features that are reproduced in nonorographic GW parameterizations when the launched stress is tied to the intensity of the sources. The first one is a realistic representation of momentum flux intermittency; the second one is an annual cycle of the stress due to that in the GW sources. Regarding the reproduction of momentum flux intermittency, *de la Cámara et al.* [2016] have shown that it is a crucial factor in order to simulate the stratospheric final warming in the SH with a realistic timing. In the present paper, we investigate the possible impact of the source-induced GW stress annual cycle on the middle atmospheric circulation. For this, we have conducted additional experiments in which the intermittency is prescribed, but the launched GW stress is uncoupled from the sources (i.e. GWLOG).

Our results show that including GW sources changes the seasonality of the middle atmospheric GW drag. The seasonality of the GW stress is filtered out quite rapidly with altitude, and a quite reasonable mid-latitude climate can be obtained with a scheme without sources and prescribing the GW intermittency. Regarding the global Brewer-Dobson circulation, the GWD differences between CONTROL and GWLOG lead to changes in the seasonality of the Brewer-Dobson circulation that can be up to 10%i n the NH, while in the SH the GWD variations are compensated by the resolved wave forcing. Our warmer climate simulations show that the GWD has a stronger seasonality when linked to the GW sources, but we do not find any dramatic amplification of climate change in the stratosphere due to the changes in nonorographic GWD specification. This result is consistent with *Sigmond and Scinocca* [2010], who found that the influence of the basic state on the circulation response to a warmer climate is much larger than the influence of changes in the orographic GW drag. Our conclusions here are nevertheless based on a limited set of experiments, concerning zonal and time mean diagnostics. The results we find regarding the mid-latitude variability seem to indicate a stronger sensitivity to the GW annual cycle. Longer runs are needed to address this issue in present and future climate.

Acknowledgments

This study was funded by the ANR/JPI-Climate/Belmont Forum project GOTHAM (ANR-15-JCLI-0004-01), and the European project ARISE2 (Horizon 2020, GAN653980). A. de la Cámara has been partially supported by the Advanced Study Program at The National Center for Atmospheric Research (NCAR), which is sponsored by the U.S. National Science Foundation.

References

Abalos, M., W. J. Randel, and E. Serrano (2012), Variability in upwelling across the tropical tropopause and correlations with tracers in the lower stratosphere, *Atmos. Chem.*

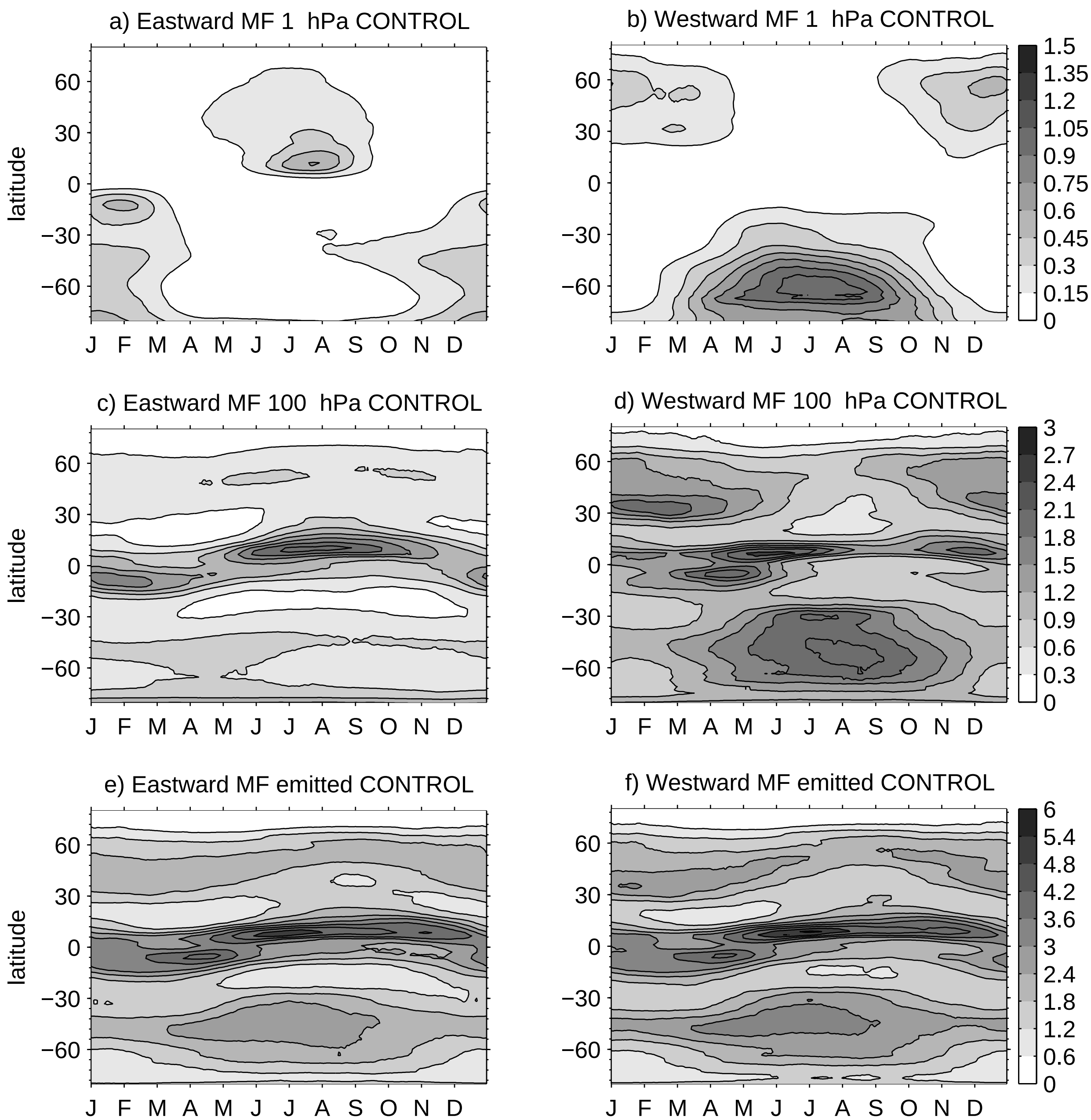

Figure 1. Total eastward (left column) and westward (right column) momentum flux at the level of emission, 100 hPa, and 1 hPa as indicated, from nonorographic gravity waves as a function of latitude and time of the year (in mPa) in CONTROL.

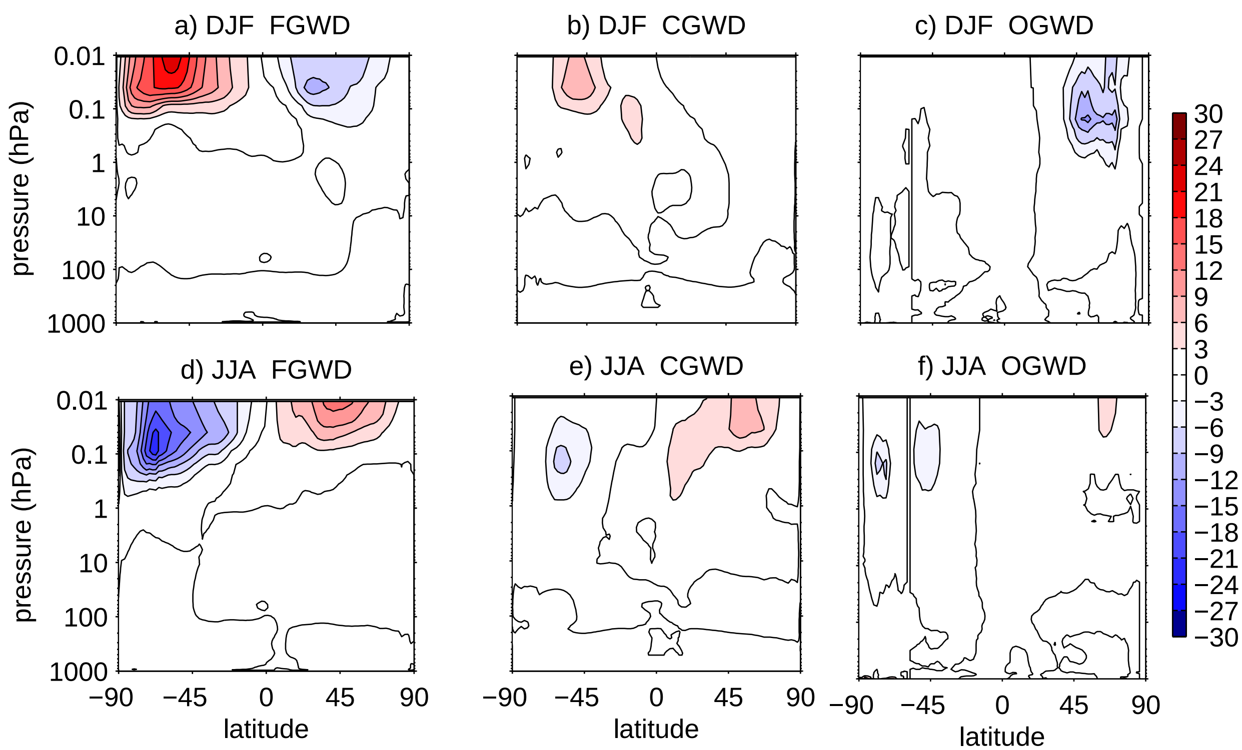

Figure 2. Longitudinally averaged drag (in m$\cdot$s$^{-1}\cdot$d^{-1}) from the frontal (FGWD, left column), convective (CGWD, central column) and orographic (OGWD, right column) gravity waves for DJF and JJA in CONTROL.

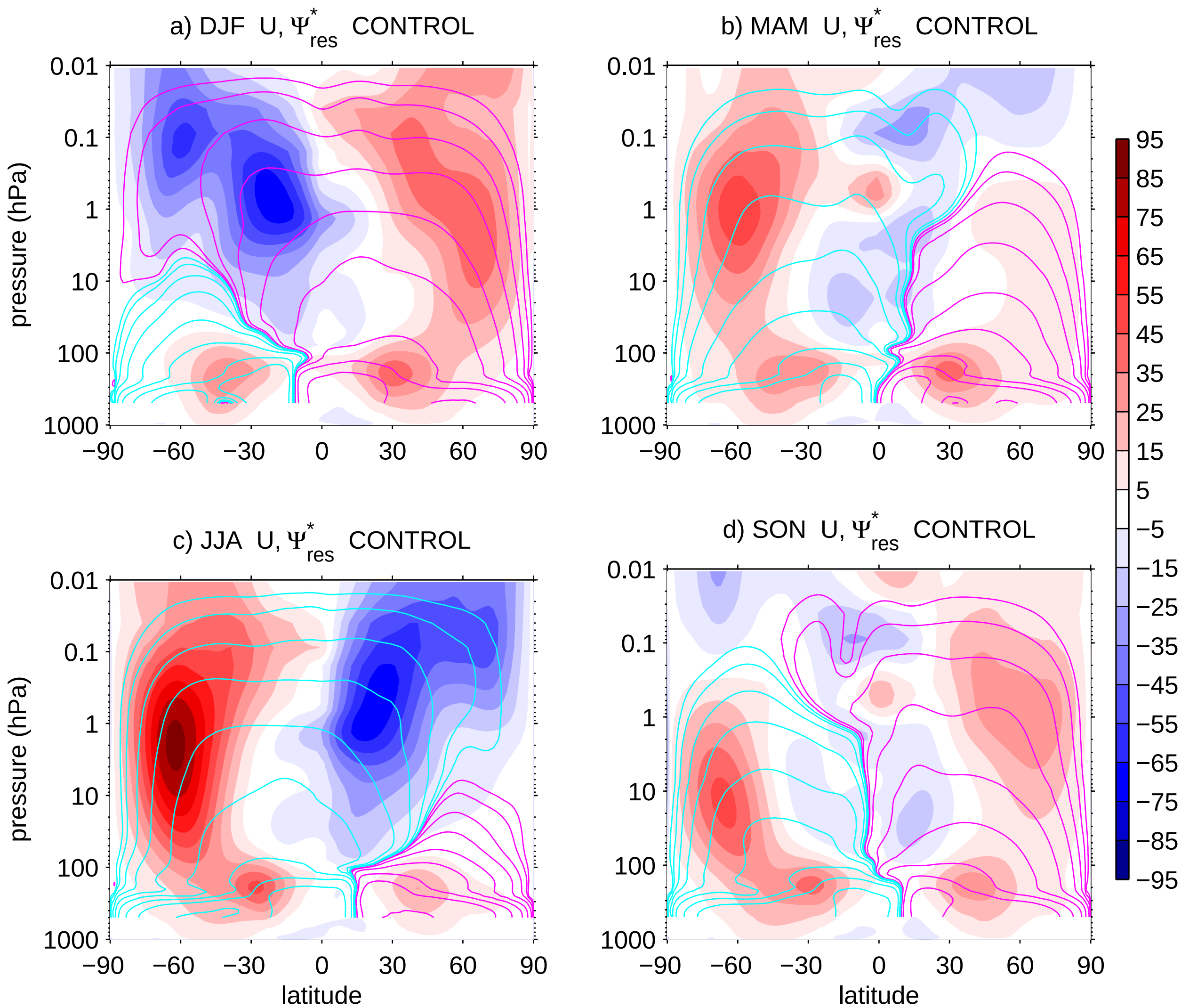

Figure 3. Zonally averaged zonal wind profiles (in m·s^{-1}, shaded), and stream function of the residual mean meridional circulation (contours) in CONTROL. Magenta contours represent positive values (i.e. clockwise circulation), and cyan contours represent negative values (i.e. counter-clockwise circulation).

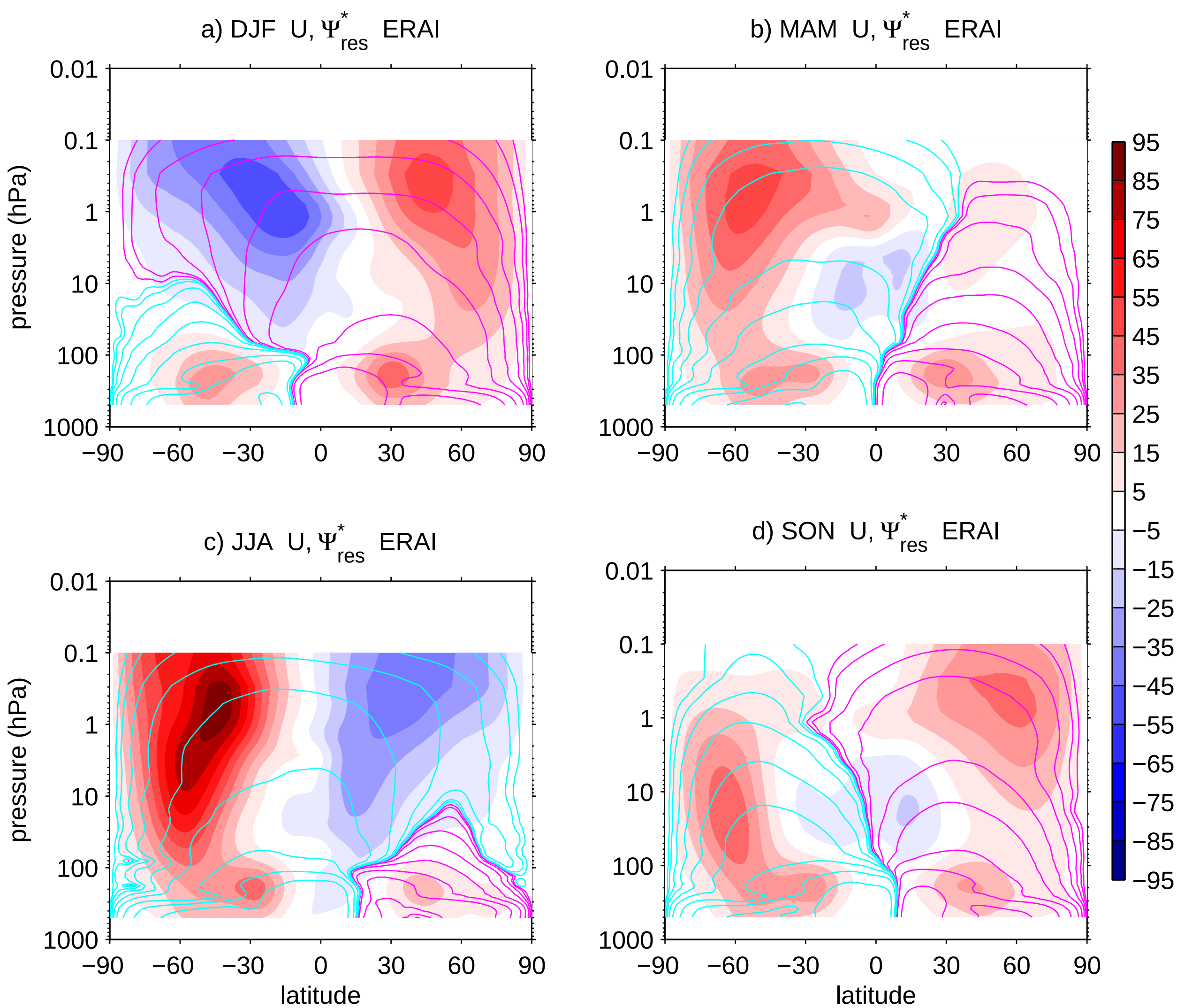

481 **Figure 4.** As in Fig. 3 but for ERA-Interim.

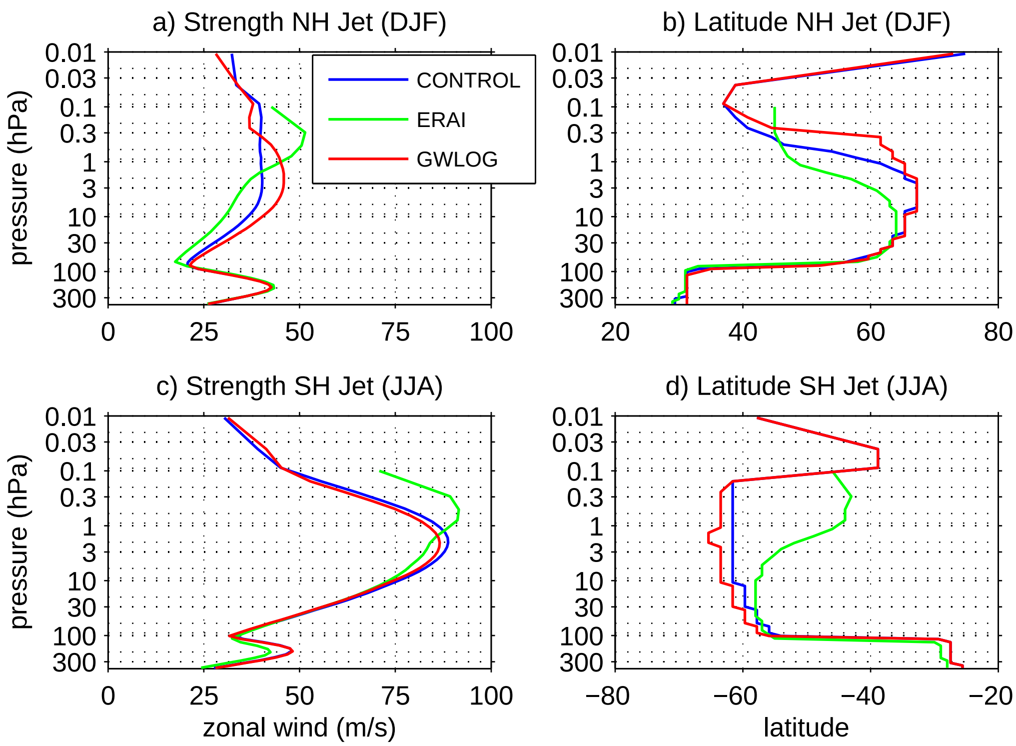

Figure 5. Zonal wind speed and latitude and latitude of the jet maxima (top) of the NH DJF climatology and (bottom) of the SH JJA climatology, for CONTROL (blue line), ERAI (green line), GWLOG (red line, see section 4).

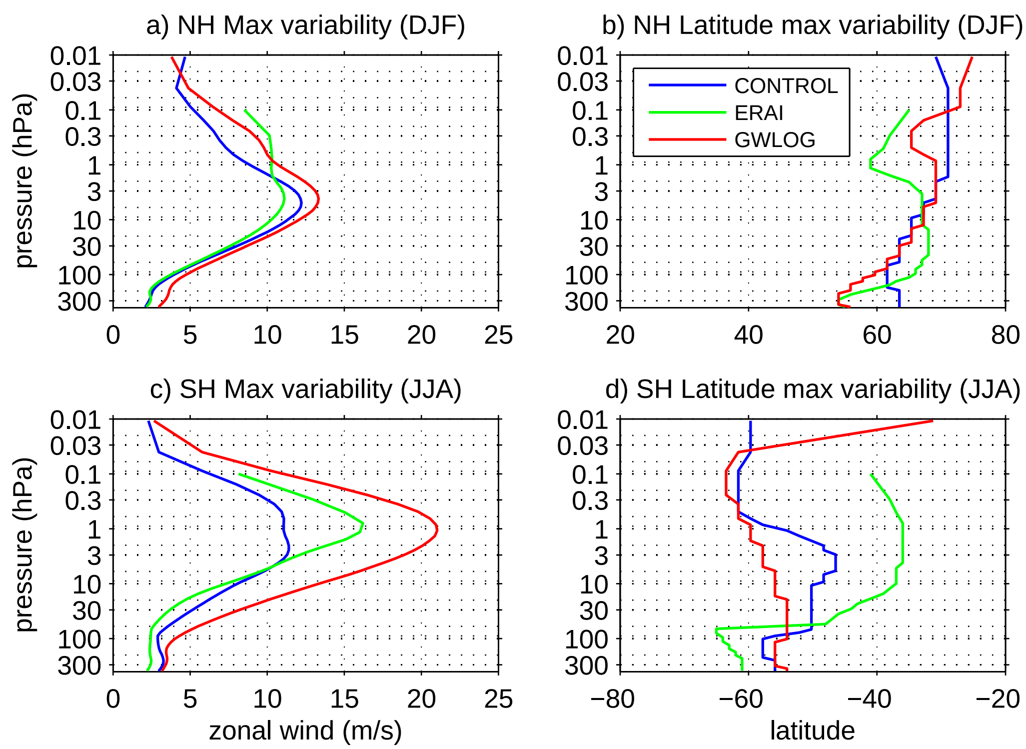

Figure 6. Location and amplitude of the maximum interannual standard deviation of the zonal mean zonal wind (top) in the NH in DJF poleward of 45°N and (bottom) in the SH in JJA poleward of 30°S, for CONTROL (blue line), ERAI (green line), GWLOG (red line, see section 4).

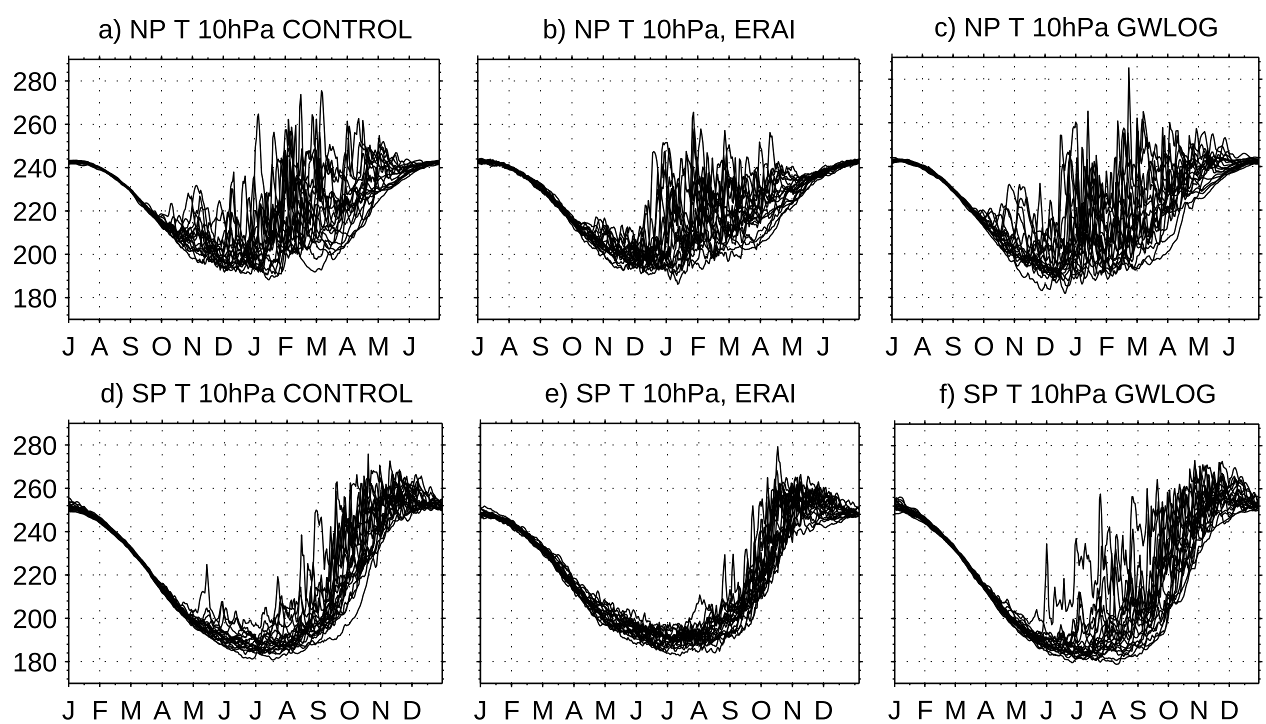

Figure 7. Polar temperatures (in K) at 10 hPa in CONTROL, ERA-Interim, and GWLOG (see section 4) for (a,b,c) the Northern Hemisphere, and (d,e,f) the Southern Hemisphere as a function of time of the year.

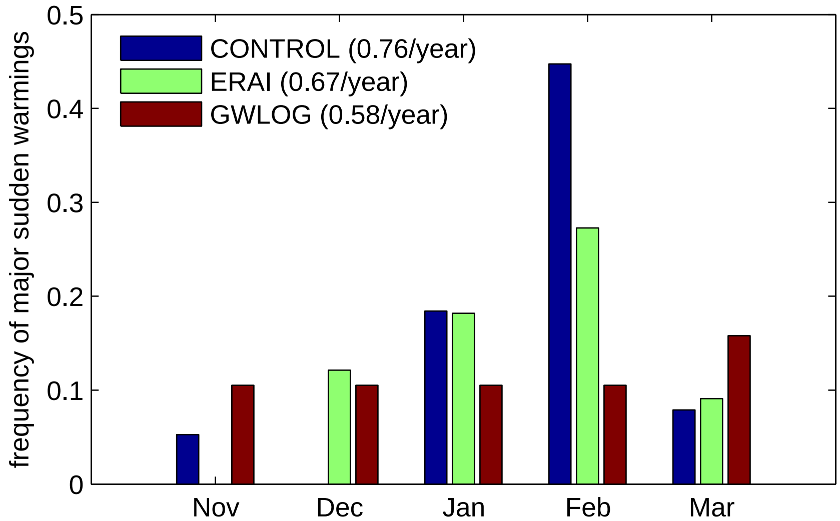

Figure 8. Frequency of major stratospheric sudden warmings (number of MSW per year) in the NH for CONTROL (blue bars), ERAI (green bars), and GWLOG (red bars, see section 4), sorted by month. The total frequency is also indicated in the figure legend.

Phys., *12*(23), 11,505–11,517, doi:10.5194/acp-12-11505-2012.

Andrews, D. G., J. R. Holton, and C. B. Leovy (1987), *Middle atmosphere dynamics*, Academic Press, 489 pp.

Beres, J. H. (2005), Implementation of a gravity wave source spectrum parameterization dependent on the properties of convection in the Whole Atmosphere Community Climate Model (WACCM), *J. Geophys. Res.*, *110*(D10), D10,108, doi: 10.1029/2004JD005504.

Bushell, A. C., N. Butchart, S. H. Derbyshire, D. R. Jackson, G. J. Shutts, S. B. Vosper, and S. Webster (2015), Parameterized Gravity Wave Momentum Fluxes from Sources Related to Convection and Large-Scale Precipitation Processes in a Global Atmosphere Model, *J. Atmos. Sci.*, *72*(11), 4349–4371, doi:10.1175/JAS-D-15-0022.1.

Butchart, N., A. J. Charlton-Perez, I. Cionni, S. C. Hardiman, P. H. Haynes, K. Krüger, P. J. Kushner, P. A. Newman, S. M. Osprey, J. Perlwitz, M. Sigmond, L. Wang, H. Akiyoshi, A. J., S. Bekki, A. Baumgaertner, P. Braesicke, C. Brühl, M. Chipperfield, M. Dameris, S. Dhomse, V. Eyring, R. Garcia, H. Garny, P. Jöckel, J.-F. Lamarque, M. Marchand, M. Michou, O. Morgenstern, T. Nakamura, S. Pawson, D. Plummer, J. Pyle, R. E., J. Scinocca, T. G. Shepherd, K. Shibata, D. Smale, H. Teyssedre, W. Tian, D. Waugh, and Y. Yamashita (2011), Multimodel climate and variability of the stratosphere, *J. Geophys. Res.*, *116*, D05,102, doi:10.1029/2010JD014995.

Charlton, A. J., and L. M. Polvani (2007), A new look at stratospheric sudden warmings. Part I: Climatology and modeling benchmarks, *J. Clim.*, *20*(3), 449–469, doi: 10.1175/JCLI3996.1.

Charron, M., and E. Manzini (2002), Gravity Waves from Fronts: Parameterization and Middle Atmosphere Response in a General Circulation Model, *J. Atmos. Sci.*, *59*(5), 923–941, doi:10.1175/1520-0469(2002)059¡0923:GWFFPA¿2.0.CO;2.

de la Cámara, A., and F. Lott (2015), A stochastic parameterization of the gravity waves emitted by fronts and jets, *Geophysical Research Letters*, *42*, 2071–2078, doi: 10.1002/GL063298.

de la Cámara, A., F. Lott, and A. Hertzog (2014), Intermittency in a stochastic parameterization of nonorographic gravity waves, *J. Geophys. Res. Atmos.*, *119*, 11,905–11,919,

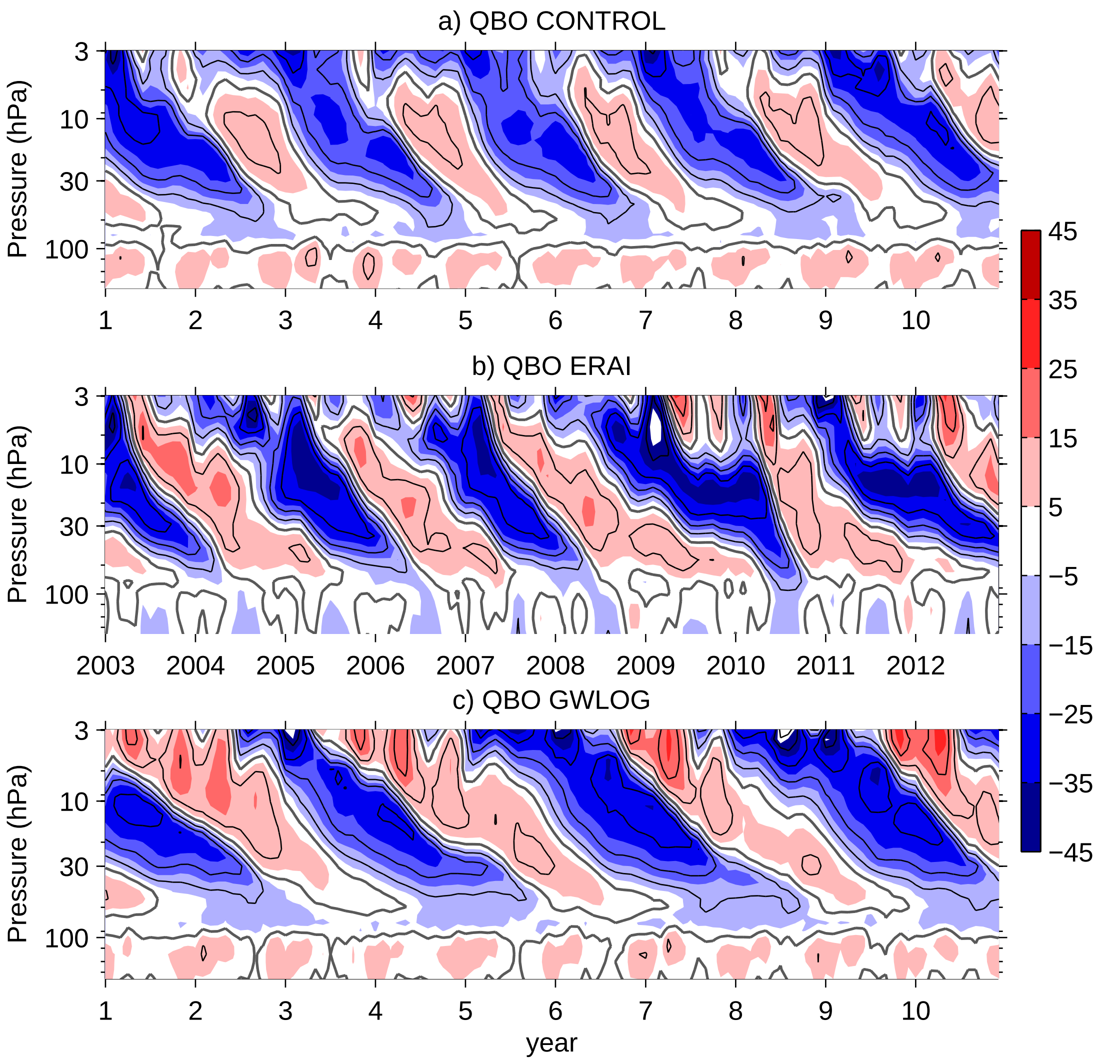

Figure 9. Zonal mean zonal wind averaged over the equatorial band 5°S5°N for (a) CONTROL, (b) ERAI, and (c) GWLOG (see section 4). Contour interval: 10 m/s, bold grey contour indicates the zero-wind line.

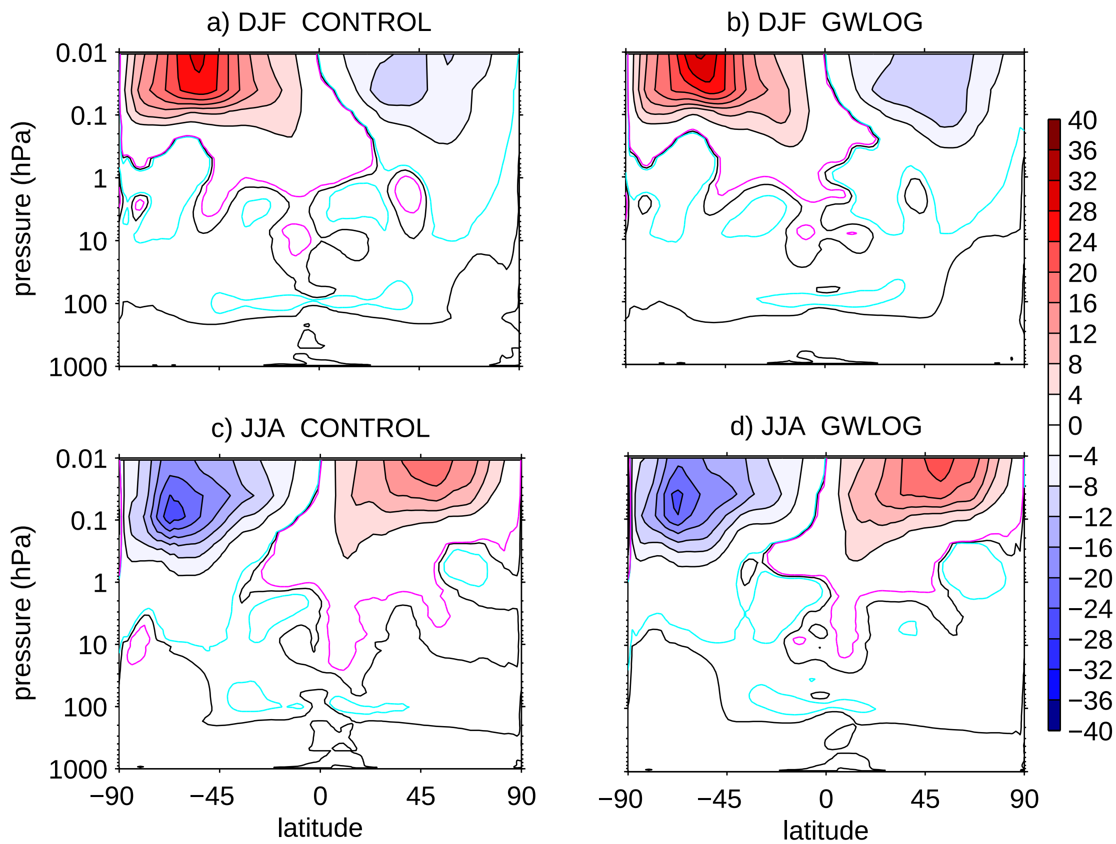

Figure 10. Zonally averaged drag from the NGW parameterizations (in m$\cdot$s$^{-1}\cdot$d^{-1}), for (a, b) DJF and (c, d) JJA, from the CONTROL and GWLOG runs as indicated. The magenta and cyan lines indicate +0.1 and -0.1 m$\cdot$s$^{-1}\cdot$d^{-1} contours, respectively.

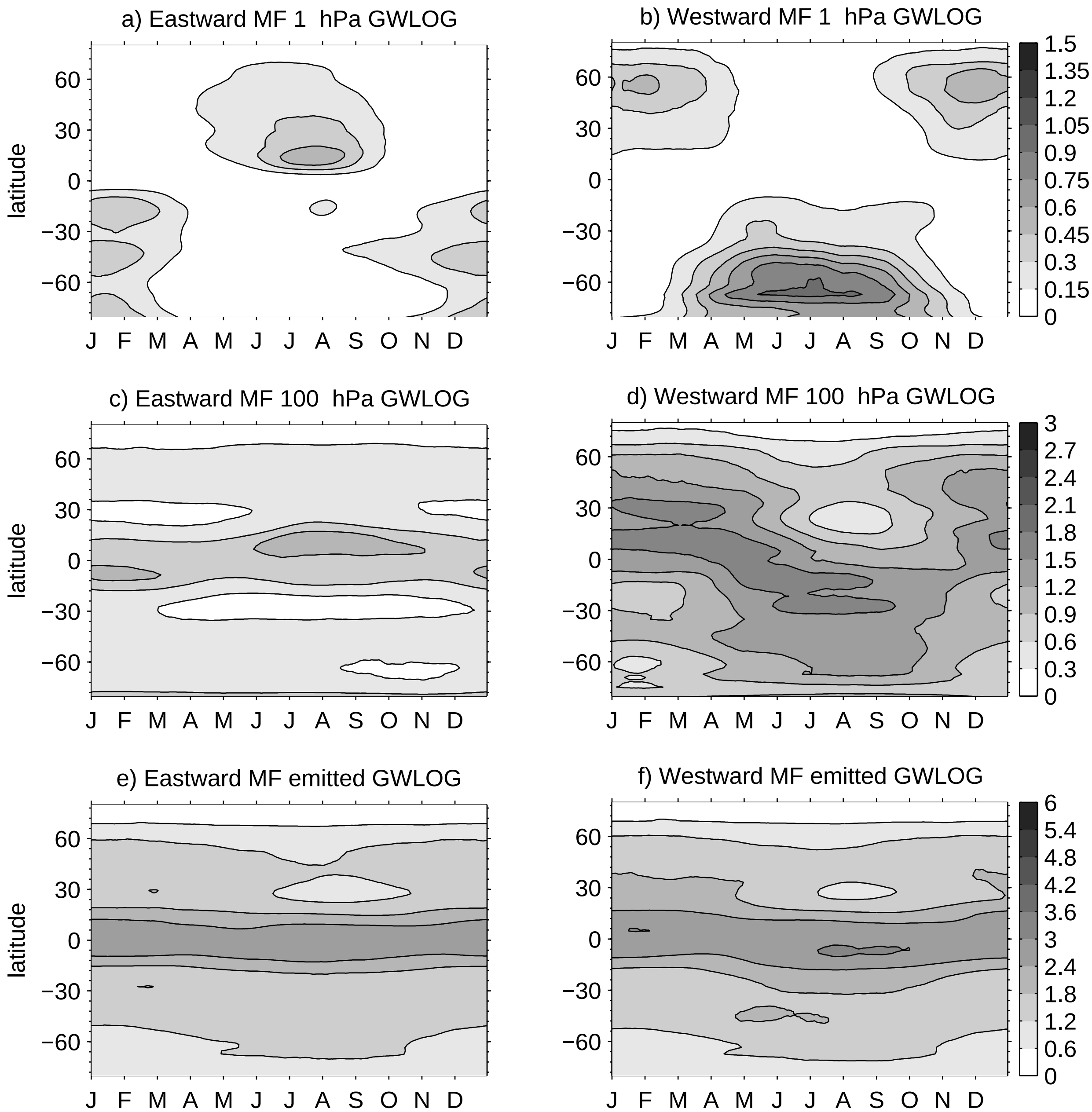

498 **Figure 11.** As in Fig. 1 but for LMDz-GWLOG.

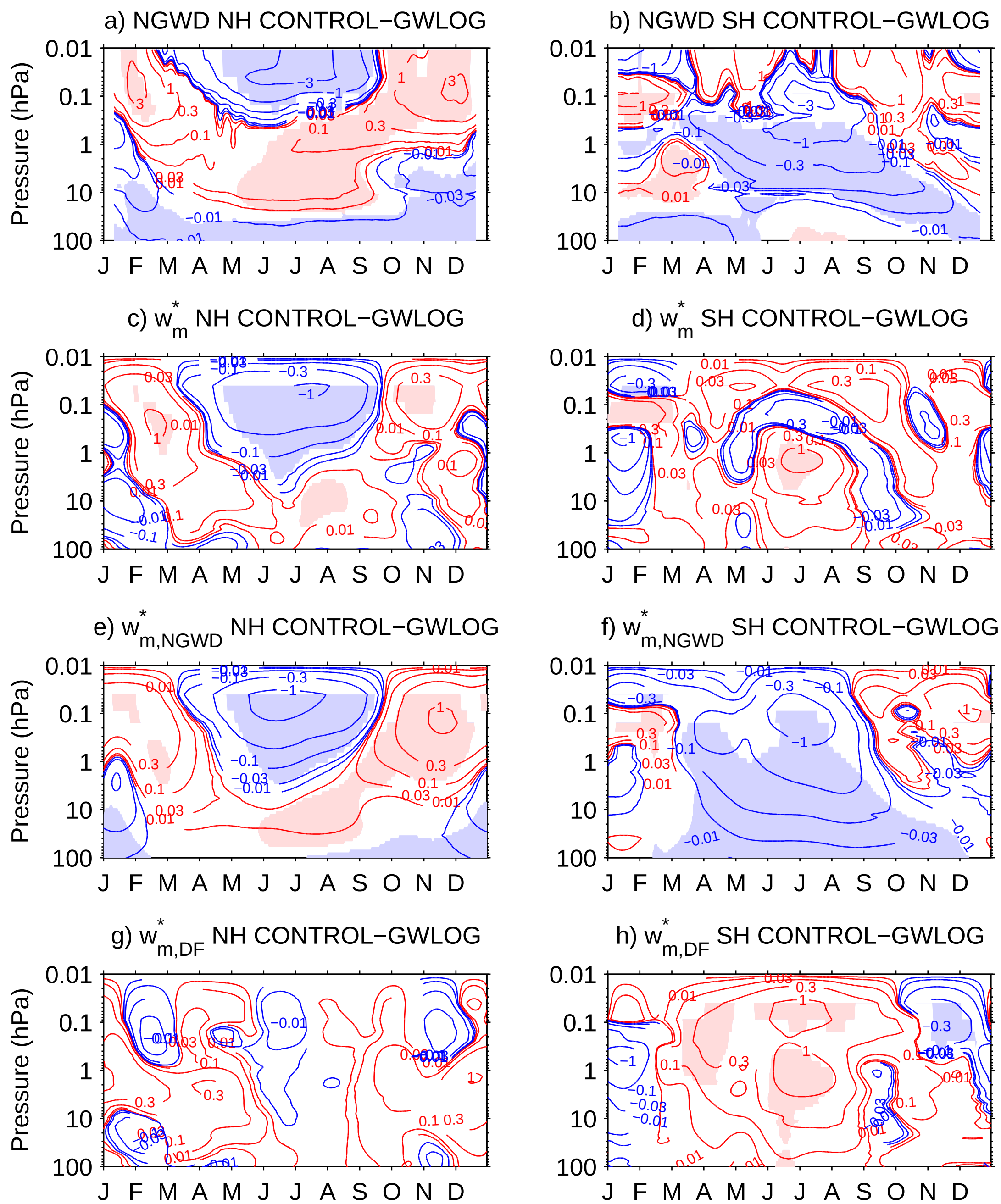

Figure 12. Differences of the vertical component of the residual mean meridional circulation derived from the TEM momentum balance equation, between the CONTROL and GWLOG runs as a function of height and time of the year. The data is longitudinally averaged over the 50°-80° latitude band in both hemispheres. Contours are at ±0.01, ±0.03, ±0.1, ±0.3, ±1, ±3 mm·s^{-1}. Light red and blue shading indicate positive and negative statistically significant differences, respectively (Student t-test, α=0.01).

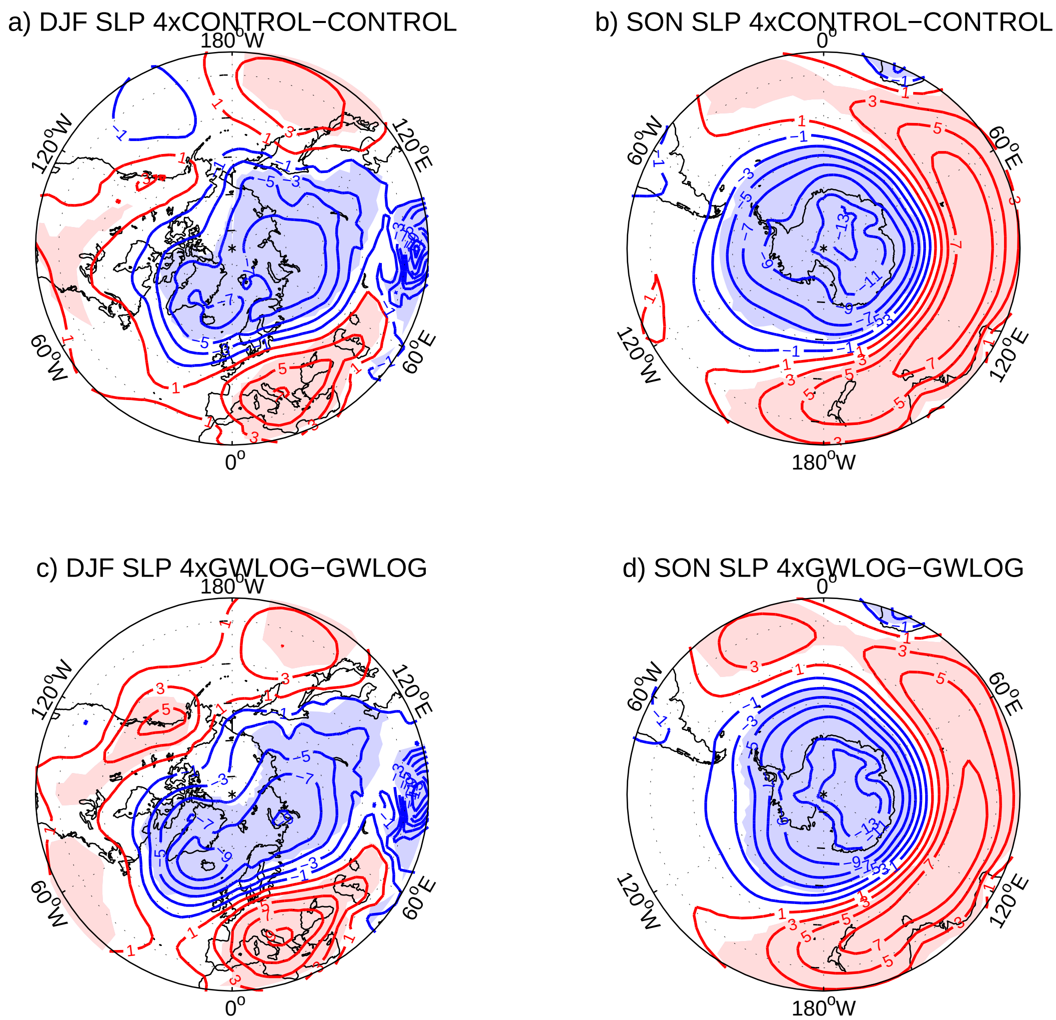

Figure 13. Differences of sea level pressure between 4xCONTROL and CONTROL, and between 4xGWLOG and GWLOG, for (a, c) DJF (in the NH), and (b, d) SON (in the SH). Contours start at ± 1 hPa, with an interval of 2 hPa. Light red and blue shadings indicate positive and negative statistically significant differences, respectively (Student t-test, α=0.01).

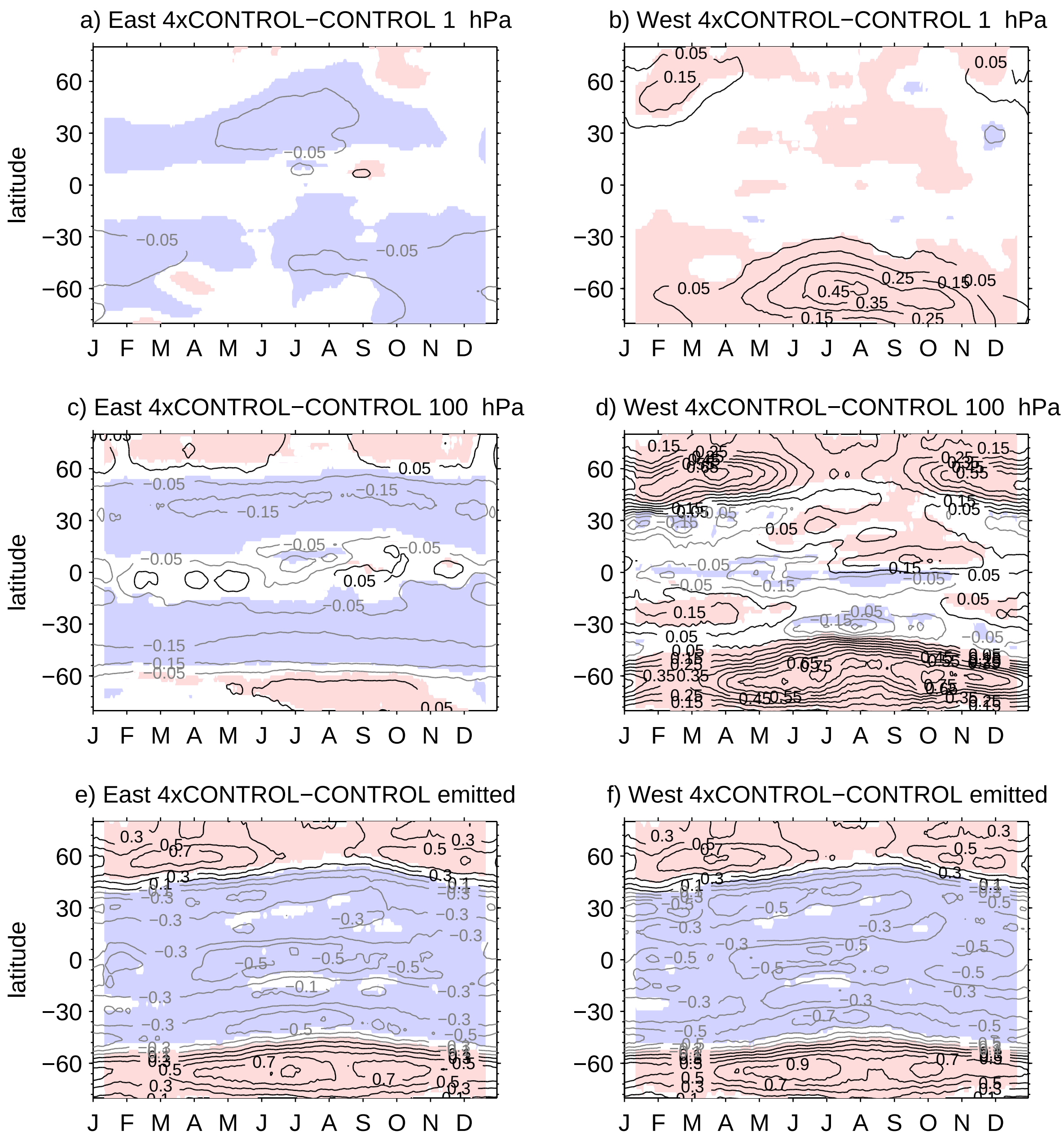

508 **Figure 14.** Differences of non-orographic eastward (left column) and westward (right column) gravity
509 wave stress (in mPa) between 4xCONTROL and CONTROL at the launching altitude, 100 hPa and 1hPa, as
510 indicated in the figure titles. Light red and blue shadings indicate positive and negative statistically significant
511 differences, respectively (Student t-test, α=0.01).

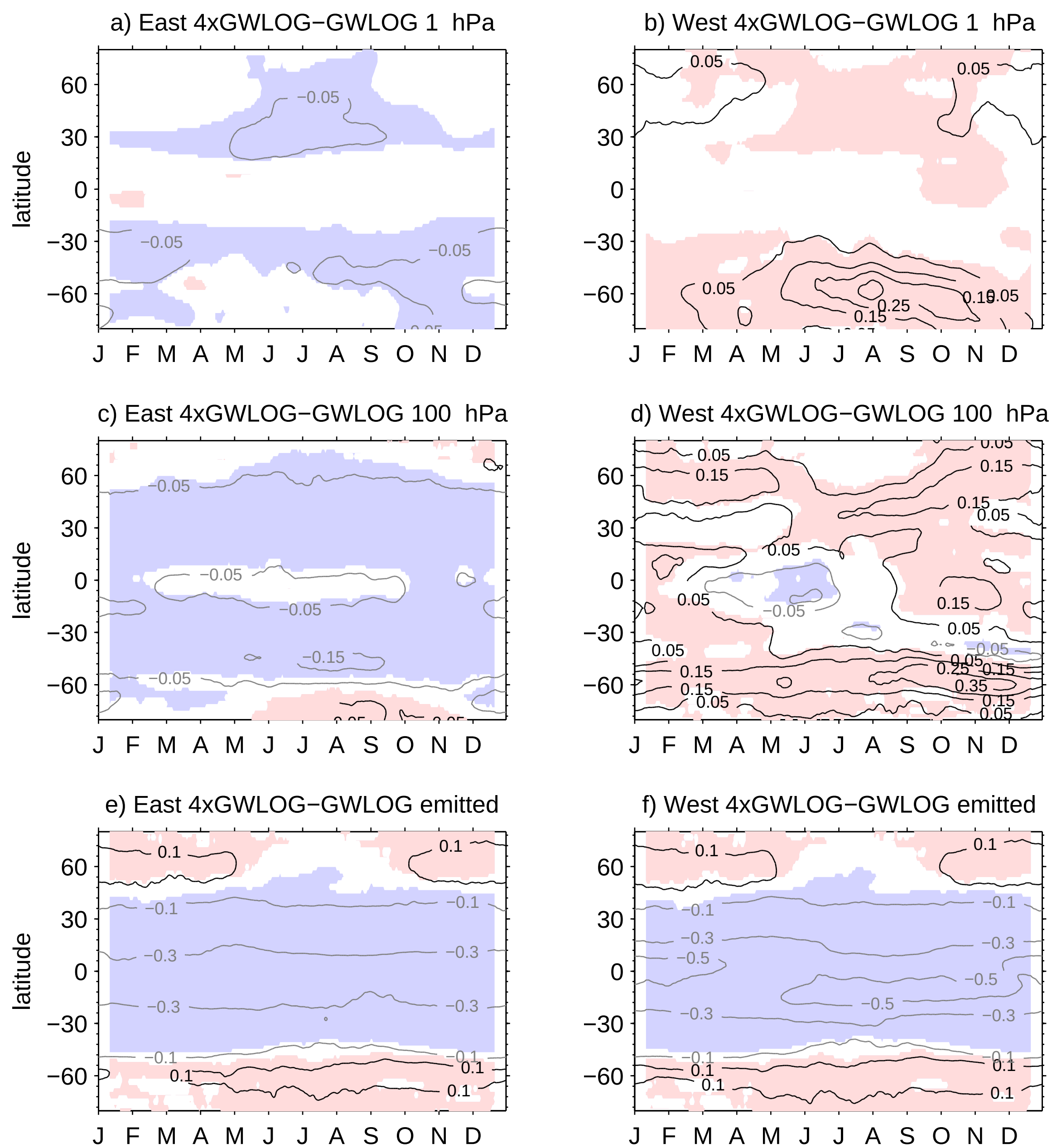

512 **Figure 15.** As in Fig. 14, but for the difference 4xGWLOG minus GWLOG.

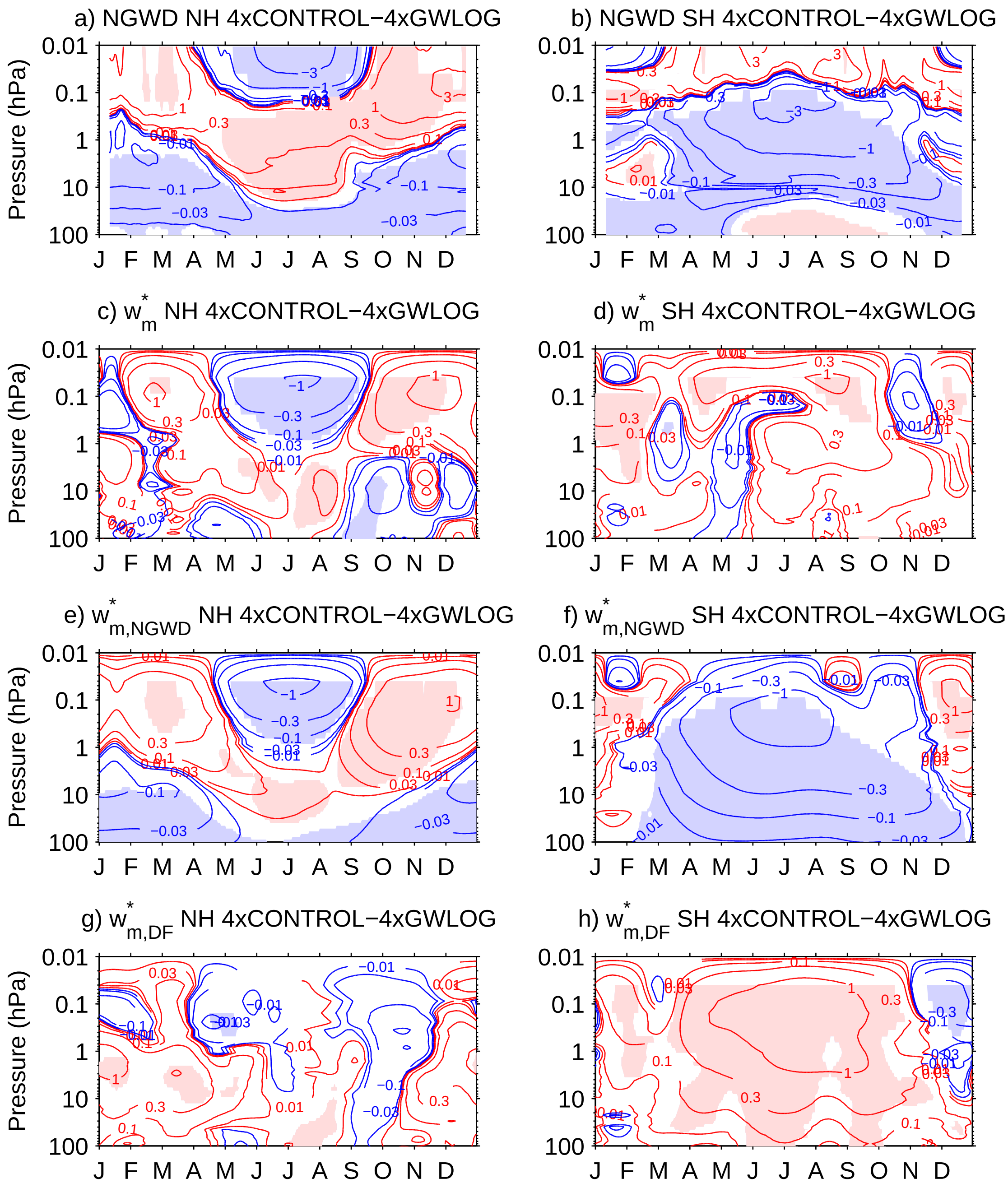

Figure 16. As in Fig. 12 but for 4xCONTROL and 4xGWLOG runs.

doi:10.1002/JD022002.

de la Cámara, A., F. Lott, V. Jewtoukoff, R. Plougonven, and A. Hertzog (2016), On the gravity wave forcing during the southern stratospheric final warming in lmdz, *J. Atmos. Sci.*, doi:10.1175/JAS-D-15-0377.1.

Eckermann, S. D. (2011), Explicitly stochastic parameterization of nonorographic gravity wave drag, *J. Atmos. Sci.*, *68*, 1749–1765, doi:10.1175/JAS3684.1.

Fritts, D. C. (1989), A review of gravity wave saturation processes, effects, and variability in the middle atmosphere, *Pure Appl. Geophys. PAGEOPH*, *130*, 343–371, doi: 10.1007/BF00874464.

Fritts, D. C., and M. J. Alexander (2003), Gravity wave dynamics and effects in the middle atmosphere, *Rev. Geophys.*, *41*(1), 1003, doi:10.1029/2001RG000106.

Hines, C. O. (1991), The Saturation of Gravity Waves in the Middle Atmosphere. Part II: Development Of Doppler-Spread Theory, doi:10.1175/1520-0469(1991)048¡1361:TSOGWI¿2.0.CO;2.

Hines, C. O. (1997), Doppler-spread parameterization of gravity-wave momentum deposition in the middle atmosphere. Part 2: Broad and quasi monochromatic spectra, and implementation, *J. Atmos. Solar-Terrestrial Phys.*, *59*(4), 387–400, doi:10.1016/S1364-6826(96)00080-6.

Jourdain, L., S. Bekki, F. Lott, and F. Lefevre (2008), The coupled chemistry-climate model LMDz-REPROBUS: description and evaluation of a transient simulation of the period 1980–1999, *Ann. Geophys.*, *26*, 1391–1413, doi:10.5194/angeo-26-1391-2008.

Lott, F. (1999), Alleviation of Stationary Biases in a GCM through a Mountain Drag Parameterization Scheme and a Simple Representation of Mountain Lift Forces, *Mon. Weather Rev.*, *127*(5), 788–801, doi:10.1175/1520-0493(1999)127¡0788:AOSBIA¿2.0.CO;2.

Lott, F., and L. Guez (2013), A stochastic parameterization of the gravity waves due to convection and its impact on the equatorial stratosphere, *J. Geophys.Res. Atmos.*, *118*, 8897–8909, doi:10.1002/jgrd.50705.

Lott, F., L. Fairhead, F. Hourdin, and P. Levan (2005), The stratospheric version of LMDz: dynamical climatologies, arctic oscillation, and impact on the surface climate, *Clim. Dyn.*, *25*(7-8), 851–868, doi:10.1007/s00382-005-0064-x.

Lott, F., R. Plougonven, and J. Vanneste (2010), Gravity Waves Generated by Sheared Potential Vorticity Anomalies, *J. Atmos. Sci.*, *67*(1), 157–170, doi:10.1175/2009JAS3134.1.

Lott, F., R. Plougonven, and J. Vanneste (2012a), Gravity Waves Generated by Sheared Three-Dimensional Potential Vorticity Anomalies, *J. Atmos. Sci.*, *69*(7), 2134–2151, doi:10.1175/JAS-D-11-0296.1.

Lott, F., L. Guez, and P. Maury (2012b), A stochastic parameterization of non-orographic gravity waves: Formalism and impact on the equatorial stratosphere, *Geophysical Research Letters*, *39*, L06,807, doi:10.1029/GL051001.

Manzini, E., N. a. McFarlane, and C. McLandress (1997), Impact of the Doppler spread parameterization on the simulation of the middle atmosphere circulation using the MA/ECHAM4 general circulation model, *J. Geophys. Res.*, *102*, 25,751, doi: 10.1029/97JD01096.

Manzini, E., A. Y. Karpechko, J. Anstey, M. P. Baldwin, R. X. Black, C. Cagnazzo, N. Calvo, B. Christiansen, P. Davini, E. Gerber, M. Giorgetta, L. Gray, S. C. Hardiman, Y. Lee, D. R. Marsh, B. A. Mcdaniel, A. Purich, A. A. Scaife, D. Shindell, S. Son, S. Watanabe, and G. Zappa (2014), Northern winter climate change: Assessment of uncertainty in CMIP5 projections related to stratosphere-troposphere coupling, *J. Geophys. Res. Atmos.*, *119*(13), 7979–7998, doi:10.1002/2013JD021403.

Maury, P., F. Lott, L. Guez, and J.-P. Duvel (2013), Tropical variability and stratospheric equatorial waves in the IPSLCM5 model, *Clim. Dyn.*, *40*(9-10), 2331–2344, doi:10.1007/s00382-011-1273-0.

McFarlane, N. A. (1987), The effect of orographically excited gravity wave drag on the general circulation of the lower stratosphere and troposphere, *J. Atmos. Sci.*, *44*, 1775–

1800, doi:http://dx.doi.org/10.1175/1520-0469(1987)044¡1775:TEOOEG¿2.0.CO;2.
McLandress, C., T. G. Shepherd, S. Polavarapu, and S. R. Beagley (2012), Is Missing Orographic Gravity Wave Drag near 60S the Cause of the Stratospheric Zonal Wind Biases in ChemistryClimate Models?, *J. Atmos. Sci.*, *69*(3), 802–818, doi:10.1175/JAS-D-11-0159.1.
Palmer, T. N., G. J. Shutts, and R. Swinbank (1986), Alleviation of a systematic westerly bias in general circulation and numerical weather prediction models through an orographic gravity wave drag parametrization, *Q. J. R. Meteorol. Soc.*, *112*(474), 1001–1039, doi:10.1002/qj.49711247406.
Randel, W. J., R. R. Garcia, and F. Wu (2002), Time-dependent upwelling in the tropical lower stratosphere estimated from the zonal-mean momentum budget, *J.Atmos. Sci.*, *59*, 2141–2152, doi:10.1175/1520-0469(2002)059¡2141:TDUITT¿2.0.CO;2.
Richter, J. H., F. Sassi, and R. R. Garcia (2010), Toward a Physically Based Gravity Wave Source Parameterization in a General Circulation Model, *J. Atmos. Sci.*, *67*(1), 136–156, doi:10.1175/2009JAS3112.1.
Rind, D., R. Suozzo, N. K. Balachandran, A. Lacis, and G. Russell (1988), The giss global climate-middle atmosphere model. part i: Model structure and climatology, *J. Atmos. Sci.*, *45*(3), 329–370, doi:10.1175/1520-0469(1988)045¡0329:TGGCMA¿2.0.CO;2.
Sassi, F., R. R. Garcia, B. A. Boville, and H. Liu (2002), On temperature inversions and the mesospheric surf zone, *J. Geophys. Res.*, *107*(D19), 4380, doi:10.1029/2001JD001525.
Scaife, A. a., T. Spangehl, D. R. Fereday, U. Cubasch, U. Langematz, H. Akiyoshi, S. Bekki, P. Braesicke, N. Butchart, M. P. Chipperfield, A. Gettelman, S. C. Hardiman, M. Michou, E. Rozanov, and T. G. Shepherd (2012), Climate change projections and stratosphere-troposphere interaction, *Clim. Dyn.*, *38*(9-10), 2089–2097, doi:10.1007/s00382-011-1080-7.
Schirber, S., E. Manzini, and M. J. Alexander (2014a), A convection-based gravity wave parameterization in a general circulation model: Implementation and improvements on the QBO, *J. Adv. Model. Earth Syst.*, *6*(1), 264–279, doi:10.1002/2013MS000286.
Schirber, S., E. Manzini, T. Krismer, and M. Giorgetta (2014b), The quasi-biennial oscillation in a warmer climate: sensitivity to different gravity wave parameterizations, *Clim. Dyn.*, pp. 825–836, doi:10.1007/s00382-014-2314-2.
Sigmond, M., and J. F. Scinocca (2010), The Influence of the Basic State on the Northern Hemisphere Circulation Response to Climate Change, *J. Clim.*, *23*(6), 1434–1446, doi:10.1175/2009JCLI3167.1.
Song, I.-S., and H.-Y. Chun (2005), Momentum flux spectrum of convectively forced internal gravity waves and its application to gravity wave drag parameterization: Part i. theory, *J. Atmos. Sci.*, *62*, 107–124.
Stephan, C., and M. J. Alexander (2015), Realistic simulations of atmospheric gravity waves over the continental U.S. using precipitation radar data, *J. Adv. Model. Earth Syst.*, *7*(2), 823–835, doi:10.1002/2014MS000396.
Warner, C. D., and M. E. McIntyre (1996), On the propagation and dissipation of gravity wave spectra through a realistic middle atmosphere, *J. Atmos. Sci.*, *53*, 3213–3235.
Wilcox, L. J., and A. J. Charlton-Perez (2013), Final warming of the southern hemisphere polar vortex in high- and low-top cmip5 models, *Journal of Geophysical Research Atmospheres*, *118*, 2535–2546, doi:10.1002/jgrd.50254.
Zülicke, C., and D. Peters (2008), Parameterization of Strong Stratospheric InertiaGravity Waves Forced by Poleward-Breaking Rossby Waves, *Mon. Weather Rev.*, *136*(1), 98–119, doi:10.1175/2007MWR2060.1.